International Journal of Robotics and Control Systems
Vol. 4, No. 4, 2024, pp. 1886-1902
ISSN 2775-2658
http://pubs2.ascee.org/index.php/ijrcs

Enhanced RSA Optimized TID Controller for Frequency Stabilization in a Two-Area Power System

Serdar Ekinci [a,1], Erdal Eker [b,2], Davut Izci [a,c,3], Aseel Smerat [d,e,4], Laith Abualigah [f,5,*]

[a] Department of Computer Engineering, Batman University, Turkey
[b] Vocational School of Social Sciences, Muş Alparslan University, Muş 49250, Turkey
[c] Applied Science Research Center, Applied Science Private University, Amman 11931, Jordan
[d] Centre for Research Impact & Outcome, Chitkara University Institute of Engineering and Technology, Chitkara University, Rajpura, 140401, Punjab, India
[e] Department of Biosciences, Saveetha School of Engineering, Saveetha Institute of Medical and Technical Sciences, Chennai 602105, India
[f] Computer Science Department, Al al-Bayt University, Mafraq 25113, Jordan
[1] serdar.ekinci@batman.edu.tr; [2] e.eker@alparslan.edu.tr; [3] davutizci@gmail.com; [4] smerat.2020@gmail.com;
[5] aligah.2020@gmail.com
* Corresponding Author

ARTICLE INFO

Article history
Received September 20, 2024
Revised October 27, 2024
Accepted November 06, 2024

Keywords
Load Frequency Control;
Reptile Search Algorithm;
Logarithmic Spiral Search;
Lévy Flight Search;
Tilt-Integral-Derivative Controller;
Renewable Energy;
Optimization Techniques

ABSTRACT

This study presents an enhanced reptile search algorithm (ImRSA) optimized tilt-integral-derivative (TID) controller for load frequency control (LFC) in a two-area power system consisting of photovoltaic (PV) and thermal power units. The ImRSA integrates Lévy flight and logarithmic spiral search mechanisms to improve the balance between exploration and exploitation, resulting in more efficient optimization performance. The proposed controller is tested against the original reptile search algorithm (RSA) and other state-of-the-art optimization methods, such as modified grey wolf optimization with cuckoo search, black widow optimization, and gorilla troops optimization. Simulation results show that the ImRSA-optimized TID controller outperforms these approaches in terms of undershoot, overshoot, settling time, and the integral of time-weighted absolute error metric. Additionally, the ImRSA demonstrates robustness in managing frequency deviations caused by solar radiation fluctuations in PV systems. The results highlight the superior efficiency and reliability of the proposed method, especially for renewable energy integration in modern power systems.

1. Introduction

Load frequency control (LFC) plays a crucial role in maintaining the stability of power systems, especially in multi-area systems where frequency deviations can propagate across interconnected grids [1]-[3]. In modern power systems, the increasing penetration of renewable energy sources, such as photovoltaic (PV) units, adds further complexity due to the intermittent and variable nature of renewable energy generation. These variations in generation can lead to significant fluctuations in system frequency and power flow, which, if not properly controlled, can compromise the stability and reliability of the entire grid.

LFC is crucial for maintaining the stability and reliability of power systems by ensuring that frequency deviations remain within permissible limits despite load variations and disturbances. The increasing integration of renewable energy sources and the presence of nonlinearities in modern power systems have intensified the need for advanced control strategies and optimization techniques. Recent studies have focused on developing sophisticated controllers optimized by various algorithms to enhance LFC performance. Sahu et al. [4] proposed an effective LFC approach using a two-degree-of-freedom tilt-integral-derivative (TID) controller optimized with the whale optimization algorithm. Their method demonstrated superior dynamic response and robustness compared to traditional PID controllers. Ekinci et al. [5] investigated the automatic generation control of a hybrid PV and reheat thermal power system using the RIME algorithm. The RIME-optimized controller effectively managed frequency deviations, showcasing improved stability in systems with renewable energy integration. Similarly, Andic et al. [6] introduced a novel sea horse optimizer-based LFC for a two-area power system comprising PV and thermal units. Their controller outperformed conventional methods, offering enhanced frequency regulation. Addressing system nonlinearities, an optimal α-variable model-free adaptive barrier function fractional-order nonlinear sliding mode control was developed for a four-area interconnected hybrid power system in a study [7]. This approach effectively handled nonlinearities and uncertainties, improving overall system stability. The application of fractional-order controllers has gained attention due to their flexibility in tuning and superior performance. Ekinci et al. [8] utilized a spider wasp optimizer to fine-tune a cascaded fractional-order controller for LFC in a PV-integrated two-area system. The optimized controller achieved better settling times and reduced overshoot, highlighting the benefits of fractional-order control. Sharma and Singh [9] explored LFC in connected multi-area multi-source power systems using energy storage devices and a lyrebird optimization algorithm-tuned PID controller. Their study demonstrated that integrating energy storage enhances frequency regulation and system resilience against disturbances.

Nature-inspired optimization algorithms have been increasingly adopted for controller tuning in LFC applications. Hassan et al. [10] applied hybrid sine cosine optimizer and balloon effect identifier algorithms for adaptive LFC in microgrids considering PV sources and electric vehicles. Their method adeptly managed the impacts of renewable integration and EV penetration on frequency stability. Younis et al. [11] enhanced LFC in interconnected power systems using a hybrid particle swarm optimization–artificial hummingbird algorithm. The hybrid approach achieved better convergence rates and control performance compared to individual optimization techniques. Further advancements include the work by Ekinci et al. [12], who presented frequency regulation of a PV-reheat thermal power system using a novel hybrid educational competition optimizer combined with pattern search and a cascaded PDN-PI controller. Their approach resulted in significant improvements in dynamic response and system stability. Apart from those studies, it is feasible to encounter more studies which are reported in [13]-[25].

In light of the challenges posed by renewable energy integration and the limitations of traditional control methods, this study proposes an enhanced reptile search algorithm (ImRSA)-optimized TID controller for LFC in a two-area power system. The ImRSA is an improved version of the original reptile search algorithm (RSA) [26], incorporating two powerful exploration mechanisms: Lévy flight [27] and logarithmic spiral search [28]. The reason of adopting the RSA as the base algorithm for the improvement stems from its demonstrated capability for various engineering problems [29]-[38]. These mechanisms improve the balance between exploration and exploitation, enabling the algorithm to more effectively search for optimal control parameters. The TID controller [39], optimized by the ImRSA, is designed to minimize frequency deviations and tie-line power fluctuations, ensuring stable and reliable operation of the power system.

The proposed ImRSA was initially tested against several benchmark functions [40]. Across all tested benchmark functions, the ImRSA consistently outperformed the original RSA in terms of both solution accuracy and consistency. The enhancements brought by the integration of Lévy flight and logarithmic spiral search mechanisms allow the ImRSA to balance global and local search strategies more effectively. In particular, the Lévy flight mechanism enables large, random jumps that improve exploration, while the logarithmic spiral search promotes convergence toward the best solution by

enhancing exploitation. The effectiveness of the proposed ImRSA-optimized TID controller was validated through a series of simulations. The results were compared with those of the original RSA and other state-of-the-art optimization techniques, such as the modified grey wolf optimization with cuckoo search algorithm-optimized TID [41], black widow algorithm-optimized PID [42] and gorilla troops algorithm-optimized PI [43]. The ImRSA demonstrated superior performance, achieving a 13% reduction in the integral of time-weighted absolute error [44] compared to RSA. It also delivered faster settling times, with an undershoot of −0.1583 Hz and an overshoot of 0.0286 Hz in Area I, outperforming both RSA and the other tested methods. Moreover, the robustness of the ImRSA-optimized TID controller was further validated under conditions of solar radiation variation, simulating the impact of fluctuating renewable energy inputs. The controller effectively mitigated the effects of these variations, maintaining system stability and minimizing power flow deviations between the interconnected areas. In conclusion, the proposed ImRSA-optimized TID controller addresses key challenges in LFC, particularly in power systems with significant renewable energy integration. The study demonstrates that the ImRSA is a robust and efficient optimization technique that can enhance the performance of LFC controllers, ensuring stable and reliable power system operation under both normal and fluctuating conditions.

2. Reptile Search Algorithm and Its Improved Version

2.1. Reptile Search Algorithm

The reptile search algorithm (RSA) is a metaheuristic optimization method inspired by the social and hunting behaviors of crocodiles [26]. The RSA can be described in three main stages: initialization, global search, and local search. During initialization, a matrix (X) of size $N \times n$ is randomly generated, where N represents the number of candidate solutions, and n represents the problem's dimensionality. Each element (candidate solution) in the matrix is generated using the following equation:

$$x_{ij} = rand \times \left(UB_j - LB_j\right) + LB_j \tag{1}$$

Here, x_{ij} is the j^{th} position of the i^{th} solution, where $i = 1, 2, \dots, N$ and $j = 1, 2, \dots, n$. In this formula, "$rand$" is a random number, and LB_j and UB_j are the lower and upper bounds for the j^{th} dimension, respectively.

In the global search phase, the RSA simulates the crocodiles' encircling behavior (high walking and belly walking) for exploration. The high walking strategy is used when $t \leq (T/4)$, where t is the current iteration and T is the maximum number of iterations. For $t \leq \left(2(T/4)\right)$ and $t > (T/4)$, the belly walking strategy is applied. The position update for the global search can be expressed as follows:

$$x_{ij}(t+1) = \begin{cases} Best_j(t) - \eta_{ij}(t) \times \beta - R_{ij}(t) \times rand; \ t \leq \dfrac{T}{4} \\ Best_j(t) \times x_{r_1 j}(t) \times ES(t) \times rand; \ t \leq 2\dfrac{T}{4} \ and \ t > \dfrac{T}{4} \end{cases} \tag{2}$$

Here, $Best_j(t)$ is the j^{th} position of the best solution found so far. The parameter β is a sensitivity factor that regulates exploration accuracy, fixed at 0.1. R_{ij} reduces the search space, and $x_{r_1 j}$ represents a random position in the i^{th} solution. The hunting operator $\eta_{ij} = Best_j(t) \times P_{ij}$, where P_{ij} denotes the percentage difference between the best and current solutions at the j^{th} position. The term $ES(t) = 2 \times r \times \left(1 - (1/T)\right)$ represents a probability factor, with r being a random integer between -1 and 1.

In addition to the global search, the RSA includes a local search phase, which simulates crocodiles' hunting behavior for exploitation, such as hunting coordination and cooperation. The local search strategy is defined as:

$$x_{ij}(t+1) = \begin{cases} Best_j(t) \times P_{ij}(t) \times rand;\ t \le 3\frac{T}{4}\ and\ t > 2\frac{T}{4} \\ Best_j(t) - \eta_{ij}(t) \times \epsilon - R_{ij}(t) \times rand;\ t \le T\ and\ t > 3\frac{T}{4} \end{cases} \quad (3)$$

Here, the hunting coordination occurs when $2T/4 \le t < 3T/4$, and hunting cooperation is performed during $3T/4 \le t < T$.

2.2. Lévy flight and Logarithmic Spiral Search Mechanisms

This work employs two enhancement techniques, Lévy flight (LF) [45] and logarithmic spiral search (LSS) [28], to boost the performance of the original RSA. The Lévy flight mechanism is effective in generating random movements within a specific search area. Lévy flight is characterized as a random process with a non-Gaussian distribution, represented by $L(s) \sim |s|^{-1-\beta}$, where β is an index ranging between 0 and 2. Mathematically, the Lévy flight distribution can be described by the following expression:

$$L(s,\gamma,\mu) = \begin{cases} \sqrt{\frac{\gamma}{2\pi}} e^{\left(-\frac{\gamma}{2(s-\mu)}\right)} \left(\frac{1}{(s-\mu)^{3/2}}\right);\ 0 < \mu < s < \infty \\ 0;\ s \le 0 \end{cases} \quad (4)$$

In this equation, s represents the sample, μ is the location parameter, and γ controls the distribution scale. A more general form of the Lévy flight distribution is expressed as:

$$F(k) = e^{\left(-\alpha|k|^{\beta}\right)}, \beta \in (0,2] \quad (5)$$

Where α is a scaling factor and β is the distribution index, as indicated in the above equation. The step length s can be determined using Eq. (6) [30]:

$$s = \left(\frac{u}{|v|^{(1/\beta)}}\right) \quad (6)$$

Here, u and v are random variables that follow a Gaussian distribution, as defined in [46].

In addition to LF, the LSS technique is also used to increase population diversity within the RSA. The LSS mechanism is illustrated in Fig. 1(a) and mathematically modeled as follows:

$$x_i^{Ls}(t) = |x_{best}(t) - x_i(t)| \cdot e^{\alpha l} \cdot \cos(2\pi l) + x_{best}(t) \quad (7)$$

In this equation, l is a random variable in the range [-1,1] (calculated as $l = 2 \times rand - 1$), α is a constant (set to 1) that shapes the spiral, and $x_{best}(t)$ represents the best solution at the current iteration. As depicted in Fig. 1(a), the LSS technique enables individuals in the population to update their positions in a spiral pattern during each iteration, converging toward the optimal solution while maintaining diversity. This enhances the algorithm's exploratory capabilities. Fig. 1(b) shows an illustration of the Lévy flight process over 100 steps, highlighting its random search behavior. By integrating LF for random movements and LSS for structured spiraling toward the target, these approaches work together to strengthen the RSA's exploration and convergence balance.

2.3. Working Mechanism of Improved RSA

The flowchart in Fig. 2 provides a detailed visual representation of the structure and working mechanism of the improved RSA (ImRSA). The ImRSA enhances the original RSA by integrating two powerful exploration strategies: Lévy flight (LF) and logarithmic spiral search (LSS), while maintaining the core stages of the RSA. The algorithm begins with the initialization phase, where a population of candidate solutions is randomly generated within predefined boundary limits. The initial parameters for the ImRSA are also set, including the sensitivity parameters $\alpha = 0.1$, $\beta = 0.1$ (for exploration accuracy in RSA), and the additional parameters specific to ImRSA, such as $P_{select} = 0.5$ (which determines the switch between LF and LSS), $b = 1$, $L = [-1, 1]$ for the logarithmic spiral

search, and $\beta = 1.5$ for Lévy flight. The fitness of each solution is then evaluated to identify the best solution.

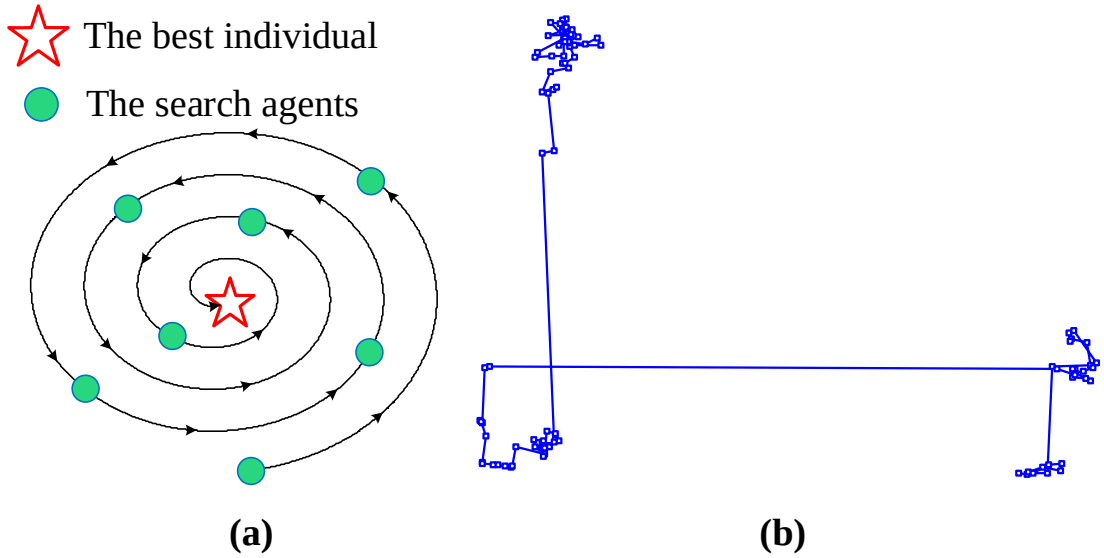

Fig. 1. Illustration of LSS (a) and LF (b) mechanisms

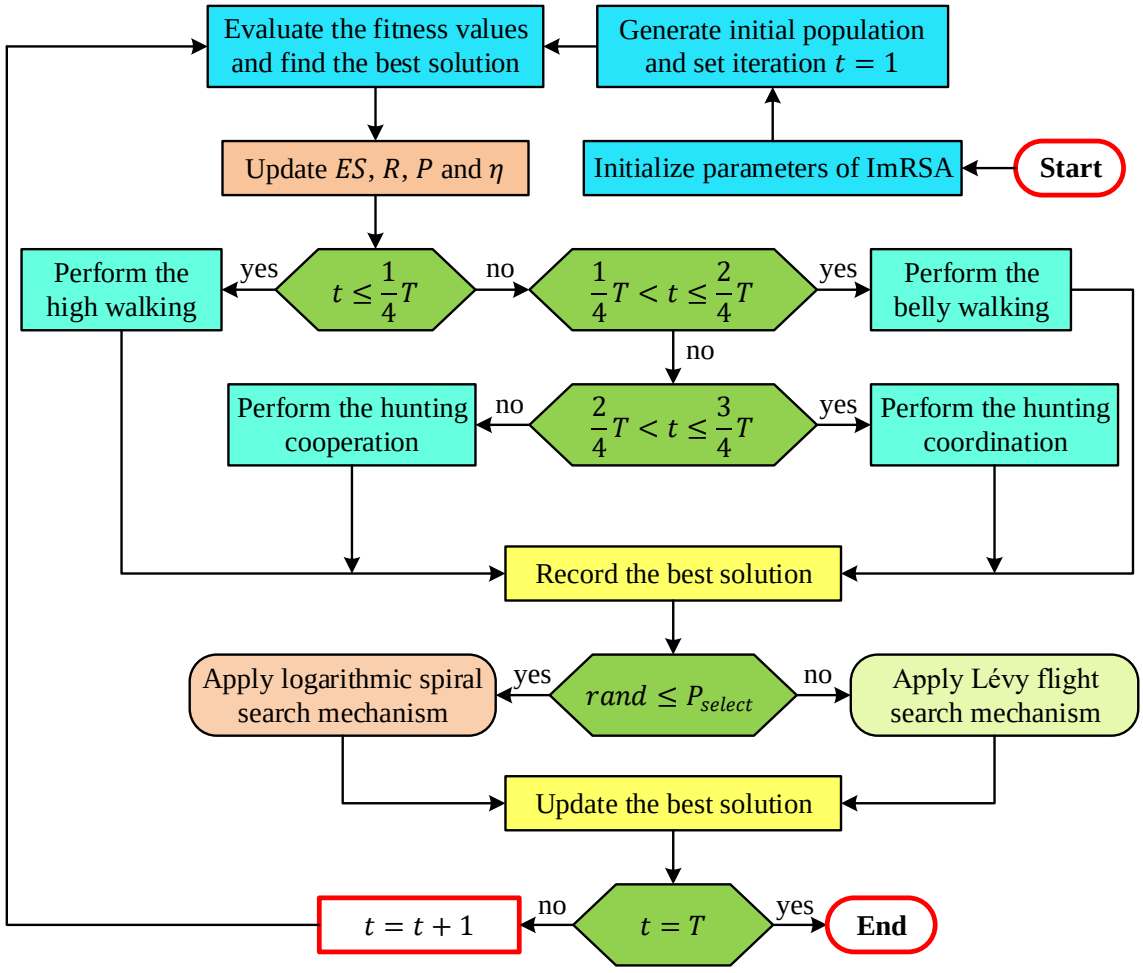

Fig. 2. Flowchart of proposed ImRSA

The global search phase is responsible for exploration. In this phase, the algorithm switches between two behaviors, high walking and belly walking, based on the current iteration t and the total

number of iterations T. High walking is performed when $t \leq (T/4)$, allowing the algorithm to focus on broader exploration. Belly walking takes over when $(T/4) < t \leq (2T/4)$, focusing on a more localized search while still maintaining some degree of exploration. During these stages, the LF and LSS mechanisms are applied to control the movement of candidate solutions, enhancing the exploration of the search space. The local search phase is focused on exploitation and refinement of the best solutions, mimicking the hunting behavior of crocodiles. It is divided into hunting coordination and hunting cooperation. Hunting coordination occurs for $(2T/4) < t \leq (3T/4)$, where candidate solutions are refined based on the current best solutions. Hunting cooperation occurs for $(3T/4) < t \leq T$, where the cooperation between solutions allows for more intensive local search, homing in on the best candidate solutions. In each iteration, the position of each candidate solution is updated. Based on a random probability, the algorithm either applies the LF or LSS mechanisms. LF is employed when $and > P_{select}$. LF facilitates large, random jumps in the search space. LSS is applied when $rand \leq P_{select}$. This mechanism ensures a more controlled, spiraling convergence toward the optimal solution while maintaining diversity in the population. The process continues until the maximum iteration is reached, at which point the algorithm records the best solution found.

3. Performance Evaluation of ImRSA on Well-Known Benchmark Functions

To evaluate the effectiveness of the ImRSA, a series of benchmark optimization functions were employed. The benchmark suite consists of widely used functions that assess the algorithm's ability to balance exploration and exploitation in both unimodal and multimodal search spaces. [40] The ImRSA was compared with the original RSA in terms of performance across these functions, and the results are tabulated in Table 1 [47]. The benchmark functions utilized include Rosenbrock, Step, Schwefel, Penalized, Kowalik, and Shekel 5 functions, each offering unique challenges in terms of dimensionality, bounds, and global optimum targets (Table 1). For each test, 30 independent runs were conducted to mitigate randomness, with a population size of 50 and a maximum iteration number of 500, ensuring robust evaluation of performance.

Table 1. Used various benchmark functions

Function	Dimension	Lower bound	Upper bound	Optimum
Rosenbrock	30	−30	30	0
Step	30	−100	100	0
Schwefel	30	−500	500	−1.2569E+04
Penalized	30	−50	50	0
Kowalik	4	−5	5	3.0749E−04
Shekel 5	4	0	10	−10.1532

The statistical performance of the ImRSA and RSA is summarized in Table 2. For each function, the best, worst, mean, and standard deviation values are recorded over the 30 independent runs. For the Rosenbrock function, the ImRSA significantly outperformed the original RSA. The ImRSA achieved a mean value of 4.7444E−16 compared to RSA's 1.8693E+01, and its standard deviation was notably lower at 2.5984E−15, highlighting its superior consistency. This suggests that the improved algorithm has a more refined balance of exploration and exploitation, allowing it to converge closer to the global optimum.

The Step function results further demonstrate the efficiency of the ImRSA. The best value obtained by the ImRSA was 6.9965E−02, a dramatic improvement over RSA's 3.8006E+00. Similarly, the mean and standard deviation values of the ImRSA, 3.4123E−01 and 1.6687E−01 respectively, reflect a marked enhancement in both performance and stability. The Schwefel function is a highly multimodal function, making it a significant challenge for any optimization algorithm. The ImRSA excelled in this test, reaching a mean value of −1.0510E+04 with a lower standard deviation compared to RSA's −5.5013E+03 mean. The ability of the ImRSA to handle complex landscapes with multiple local minima is apparent here, highlighting its exploration capabilities. For the Penalized function, the ImRSA also demonstrated substantial improvements. It achieved a best value of

1.4638E−02 and a mean of 3.7449E−02, whereas the RSA struggled, yielding a best of 4.7320E−01 and a mean of 1.2103E+00. This result indicates the ImRSA's ability to effectively exploit the search space for precision solutions. The performance on the Kowalik and Shekel 5 functions again showed that the ImRSA delivers more accurate and consistent results than RSA. In the Kowalik function, ImRSA's best result of 3.0859E−04 was closer to the optimum compared to RSA's 5.5247E−04. In the Shekel 5 function, ImRSA achieved a best result of −1.0153E+01, very close to the theoretical optimum of −10.1532.

Table 2. Statistical metrics comparison of RSA and ImRSA on benchmark functions

Function	Algorithm	Best	Worst	Mean	Standard deviation
Rosenbrock	RSA	4.6823E−24	2.8990E+01	1.8693E+01	1.3814E+01
	ImRSA	2.3546E−25	1.4232E−14	4.7444E−16	2.5984E−15
Step	RSA	3.8006E+00	7.2617E+00	6.5738E+00	9.4223E−01
	ImRSA	6.9965E−02	7.4829E−01	3.4123E−01	1.6687E−01
Schwefel	RSA	−5.6560E+03	−5.0473E+03	−5.5013E+03	1.5209E+02
	ImRSA	−1.1605E+04	−8.7883E+03	−1.0510E+04	7.9134E+02
Penalized	RSA	4.7320E−01	1.6033E+00	1.2103E+00	3.2784E−01
	ImRSA	1.4638E−02	7.5462E−02	3.7449E−02	1.7191E−02
Kowalik	RSA	5.5247E−04	3.5432E−03	1.4710E−03	6.6595E−04
	ImRSA	3.0859E−04	7.9092E−04	5.7936E−04	1.5802E−04
Shekel 5	RSA	−5.0552E+00	−5.0552E+00	−5.0552E+00	1.8067E−15
	ImRSA	−1.0153E+01	−9.9993E+00	−1.0122E+01	3.7473E−02

4. Real-World Engineering Problem: ImRSA-Optimized TID Controller for LFC

This section illustrates the application of the ImRSA to optimize a tilt-integral-derivative (TID) controller for LFC in a two-area power system consisting of PV grids and thermal power units. Effective LFC is critical to maintain frequency stability and ensure that power flows between interconnected areas remain balanced, especially when integrating renewable energy sources such as PV grids. The transfer functions of the power system model used in this study are provided in Table 3.

Table 3. Transfer functions of photovoltaic grid and thermal power units

Area I	Area II			
Photovoltaic grid	**Governor**	**Turbine**	**Reheater**	**Power system**
$G_{pv}(s)=\frac{-As+B}{s^2+Cs+D}$	$G_g(s)=\frac{K_g}{T_g s+1}$	$G_t(s)=\frac{K_t}{T_t s+1}$	$G_r(s)=\frac{K_r T_r s+1}{T_r s+1}$	$G_{ps}(s)=\frac{K_{ps}}{T_{ps} s+1}$

The TID controller is designed to optimize the frequency response and reduce power deviations between the two areas. The controller's transfer function is defined as [48]:

$$TID(s)=\frac{K_T}{s^{1/n}}+\frac{K_I}{s}+K_D s \tag{8}$$

Where K_T is the tilt term, K_I is the integral term, K_D is the derivative term, and n is a parameter that shapes the order of the tilt component. Unlike traditional PID controller [49], [50] or its filtered version [51], this TID structure enhances the controller's ability to handle both fast and slow dynamics by incorporating the tilt action, which improves system stability and damping. The performance of the TID controller is optimized by minimizing the integral of time-weighted absolute error (ITAE) objective function, which is expressed as [52]:

$$ITAE=\int_0^{t_f}(|\Delta f_1|+|\Delta f_2|+|\Delta P_{tie}|)tdt \tag{9}$$

Where Δf_1 and Δf_2 represent the frequency deviations in Areas I and II, respectively, ΔP_{tie} is the tie-line power deviation between the areas, and t_f is the final time for the simulation, set to 30 seconds. The ITAE objective function emphasizes the importance of reducing frequency and power deviations over time, ensuring that the system reaches a steady state with minimal overshoot and oscillations.

The block diagram in Fig. 3 illustrates the structure of the TID-controlled two-area PV-thermal power system. The ImRSA is employed to tune the parameters of the TID controller to minimize the ITAE value, ensuring optimal load frequency control. The key components of the system include TID controllers for the PV grid and thermal units in Areas I and II, the dynamic models of the PV grid, governor, turbine, reheater, and power system, as described by the transfer functions, and the tie-line connecting the two areas, which transfers power between them and needs to be carefully controlled to prevent instability. The ImRSA iteratively adjusts the TID controller parameters to achieve the best possible balance between minimizing frequency deviations and ensuring fast system response. This control architecture enables efficient coordination between the renewable and thermal generation sources, ensuring that frequency deviations and tie-line power fluctuations are minimized, even under varying load conditions and disturbances.

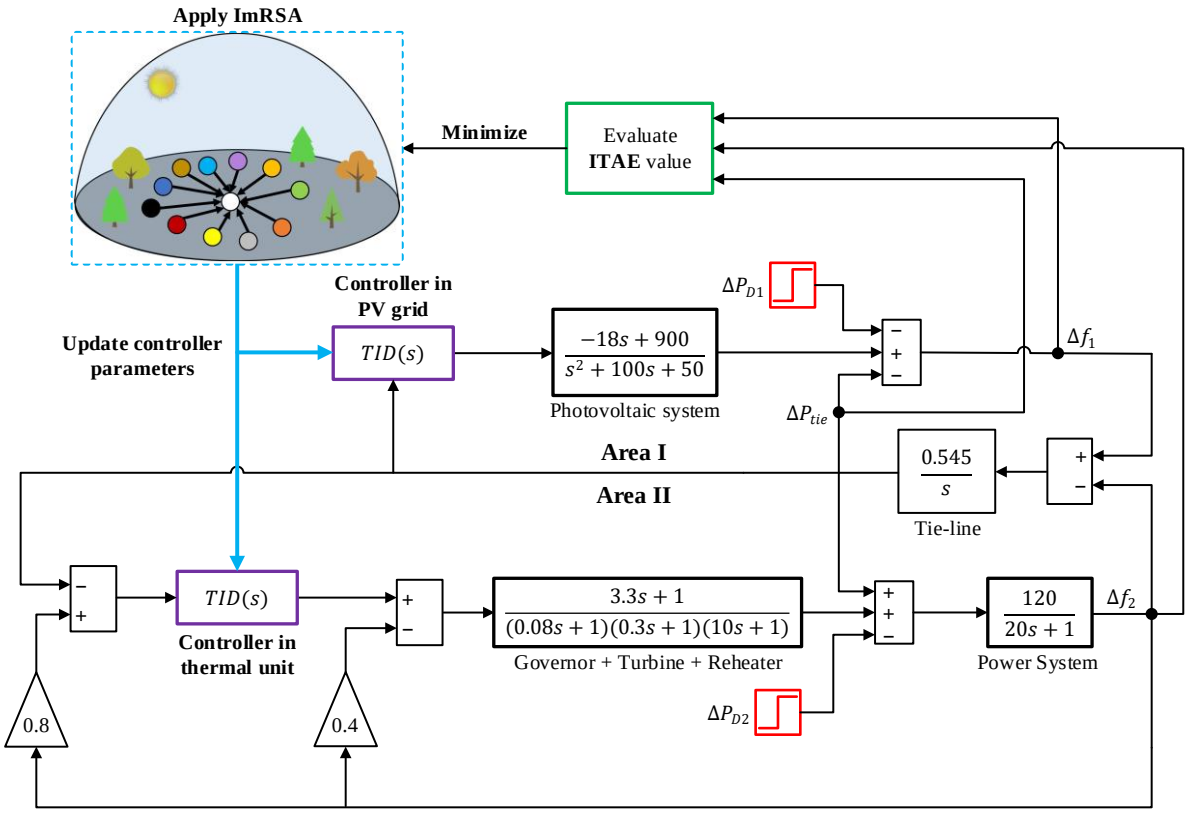

Fig. 3. Block diagram of TID controlled two-area PV-thermal system

5. Simulation Results

5.1. Statistical Analysis

In this section, the performance of the ImRSA is compared with the original RSA in the context of optimizing a TID controller for LFC. The simulations were conducted with a population size of $N = 40$ and a maximum iteration number $T = 100$. For each algorithm, 20 independent runs were performed to ensure the reliability of the results. Table 4 presents the statistical metrics (best, worst, mean, and standard deviation) of the RSA and ImRSA in the LFC optimization problem. The ImRSA consistently outperforms the RSA across all statistical measures, achieving better solutions with lower variation across the runs. As observed in the table, the best ITAE value obtained by the ImRSA was 0.8239, compared to RSA's 0.9251. Furthermore, the ImRSA showed greater consistency with a lower

standard deviation of 0.0291, indicating more consistent results across different runs compared to RSA's 0.0353. This illustrates that ImRSA offers more robust performance in optimizing LFC systems.

Table 4. Statistical metrics comparison of RSA and ImRSA on LFC optimization problem

Algorithm	Best	Worst	Mean	Standard deviation
ImRSA	0.8239	0.9416	0.8607	0.0291
RSA	0.9251	1.0659	0.9639	0.0353

The convergence behavior of the RSA and ImRSA during the LFC optimization process is illustrated in Fig. 4, which plots the ITAE against the iteration number for both algorithms. The figure clearly shows that ImRSA converges more rapidly than RSA, with ImRSA reaching lower ITAE values earlier in the optimization process. As depicted in Fig. 4, the ImRSA achieves a significantly lower ITAE value compared to RSA within the same number of iterations. The ImRSA consistently outperforms RSA in minimizing the ITAE, indicating faster convergence and more efficient optimization for LFC tasks.

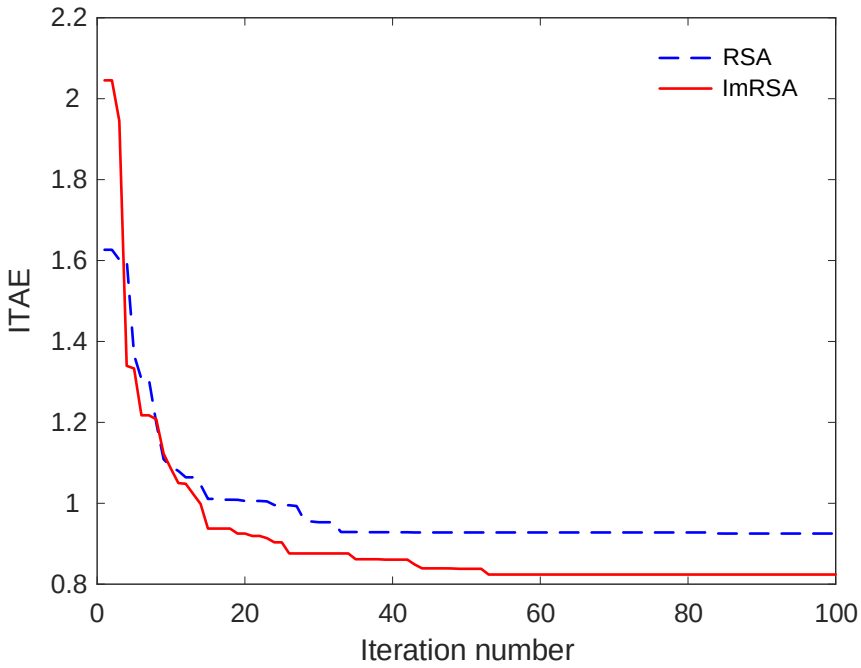

Fig. 4. Change of ITAE for RSA and ImRSA

The optimal values of the TID controller parameters for Areas I and II, obtained using both RSA and ImRSA, are summarized in Table 5. The bounds for each parameter are set between −2 and 2 for the controller gains (K_T, K_I, and K_D) and between 1 and 500 for the parameter n. As shown in Table 5, the ImRSA obtained optimized controller parameters closer to the theoretical optimum values compared to RSA.

Table 5. Bounds and optimal values for TID controller parameters

Area	Parameter	Lower bound	Upper bound	Optimized by RSA	Optimized by ImRSA
I	K_T	−2	2	−1.8484	−1.0177
	K_I	−2	2	−0.2572	−0.1584
	K_D	−2	2	−1.9977	−1.9910
	n	1	500	500.0000	488.5471
II	K_T	−2	2	−2.0000	−2.0000
	K_I	−2	2	−2.0000	−2.0000
	K_D	−2	2	−0.4936	−0.5970
	n	1	500	5.3111	5.1438

5.2. Comparison with Recently Documented Studies

This section compares the performance of the ImRSA-optimized TID controller with three advanced control strategies: the modified grey wolf optimization with cuckoo search algorithm (MGWO-CS)-optimized TID [41], black widow optimization (BWOA)-optimized PID [42] and gorilla troops optimization (GTO)-optimized PI [43]. Each of these controllers was subjected to a 10% step load change applied to both areas of a two-area power system ($\Delta P_{D1} = \Delta P_{D2} = 0.1\ pu$). The comparison is based on transient response characteristics, including undershoot, overshoot, and settling time.

Fig. 5 illustrates the transient response of frequency deviation in Area I for each controller. The ImRSA-optimized TID controller shows superior performance, with a minimal undershoot of −0.1583 Hz and overshoot of 0.0286 Hz, achieving a settling time of 1.3399 seconds. In contrast, the RSA-optimized TID controller has a slightly higher overshoot (0.0392 Hz) and faster settling time (1.2966 seconds). The MGWO-CS-optimized TID controller performs adequately but exhibits a higher overshoot and slower response compared to ImRSA. The BWOA-optimized PID and GTO-optimized PI controllers show the poorest performance, with the GTO controller displaying the highest overshoot and longest settling time of 2.7990 seconds.

As shown in Fig. 6, the frequency deviation in Area II is also better controlled by the ImRSA-optimized TID controller, with an undershoot of −0.1597 Hz and an overshoot of 0.0283 Hz. The settling time of 1.2414 seconds is the fastest among all tested controllers. The RSA-optimized TID controller achieves similar performance but with slightly worse overshoot values and a settling time of 1.2067 seconds. The MGWO-CS-optimized TID controller shows higher undershoot but acceptable settling time, while the BWOA-optimized PID and GTO-optimized PI controllers lag behind, with the GTO controller showing the slowest response time (4.0053 seconds).

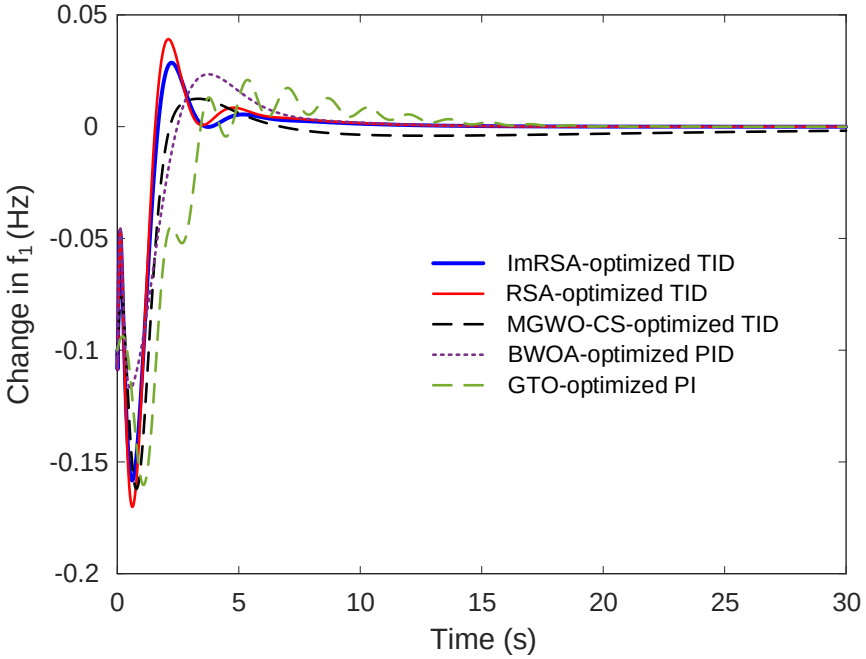

Fig. 5. Transient response of frequency deviation in Area I

Fig. 7 presents the transient response of tie-line power deviation for all controllers. The ImRSA-optimized TID controller produces the best results, with a deviation of −0.0067 puMW and no steady-state error and zero settling time. The RSA-optimized TID controller performs similarly, with a deviation of −0.0062 puMW. Both the MGWO-CS and GTO controllers show large deviations and slower recovery times, making them less suitable for effective tie-line power control.

Table 6 provides a comparison of the undershoot, overshoot, and settling time metrics for frequency deviation in Areas I and II, as well as tie-line power deviation. Settling times were

calculated using a ± 0.05 Hz tolerance band for Δf_1 and Δf_2, and a ± 0.01 puMW tolerance band for ΔP_{tie}. The ImRSA-optimized TID controller consistently achieves lower undershoot and overshoot values with faster settling times compared to the other controllers, confirming its superior performance in load frequency control.

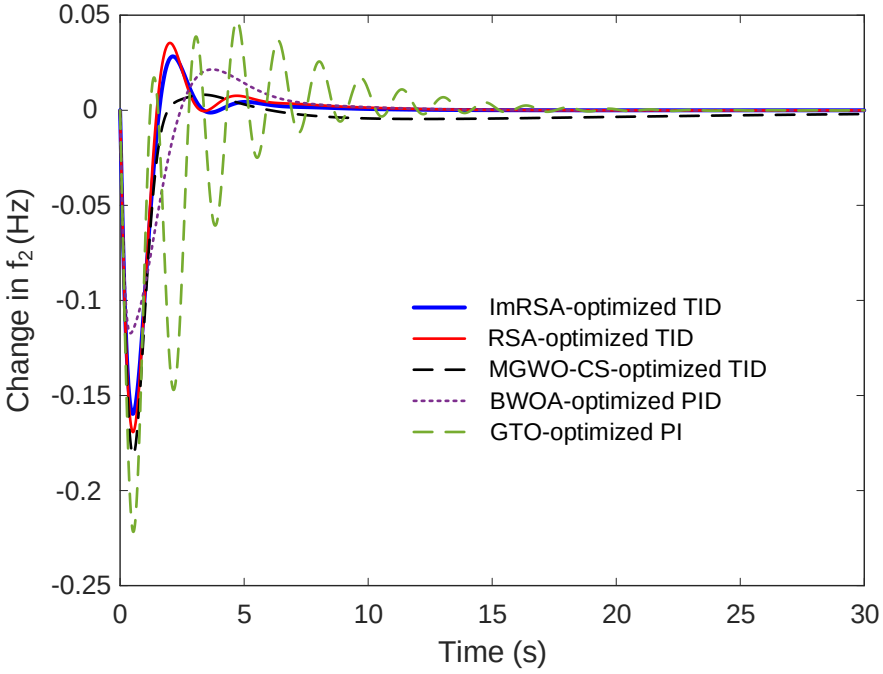

Fig. 6. Transient response of frequency deviation in Area II

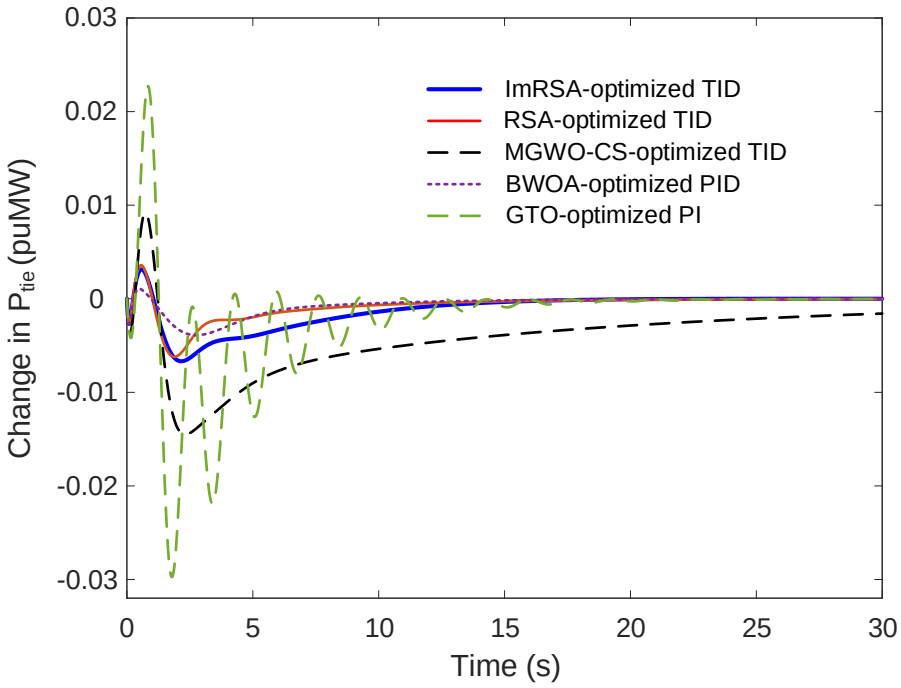

Fig. 7. Transient response of tie-line power deviation

Finally, the objective function values based on the ITAE for all controllers are provided in Table 7. The ImRSA-optimized TID controller achieves the lowest ITAE value of 0.8239, outperforming the RSA-optimized TID controller, which has an ITAE value of 0.9251. The MGWO-CS, BWOA, and GTO based controllers exhibit significantly higher ITAE values, indicating poorer overall performance.

Table 6. Undershoot (US), overshoot (OS) and settling time (t_s) metrics for various controllers

Output signal	Controller type	US	OS	t_s (s)
Δf_1 (Hz)	ImRSA-optimized TID (proposed)	−0.1583	0.0286	1.3399
	RSA-optimized TID (proposed)	−0.1701	0.0392	1.2966
	MGWO-CS-optimized TID	−0.1620	0.0125	1.5816
	BWOA-optimized PID	−0.1172	0.0234	1.6523
	GTO-optimized PI	−0.1603	0.0209	2.7990
Δf_2 (Hz)	ImRSA-optimized TID (proposed)	−0.1597	0.0283	1.2414
	RSA-optimized TID (proposed)	−0.1692	0.0354	1.2067
	MGWO-CS-optimized TID	−0.1814	0.0082	1.2810
	BWOA-optimized PID	−0.1172	0.0215	1.5783
	GTO-optimized PI	−0.2217	0.0471	4.0053
ΔP_{tie} (puMW)	ImRSA-optimized TID (proposed)	−0.0067	0.0031	0
	RSA-optimized TID (proposed)	−0.0062	0.0036	0
	MGWO-CS-optimized TID	−0.0145	0.0092	3.7363
	BWOA-optimized PID	−0.0039	0.0011	0
	GTO-optimized PI	−0.0297	0.0227	5.3183

Table 7. Comparison of $ITAE$ objective function for various controller types

Controller type	$ITAE$
ImRSA-optimized TID (proposed)	**0.8239**
RSA-optimized TID (proposed)	0.9251
MGWO-CS-optimized TID	4.5506
BWOA-optimized PID	1.2126
GTO-optimized PI	2.9185

5.3. Influence of Solar Radiation Variation in Area I

In this section, the impact of solar radiation variation on the performance of the ImRSA-optimized TID controller in Area I is evaluated. PV power generation is highly dependent on solar radiation, and any fluctuations can affect the frequency stability and tie-line power balance in interconnected power systems. The ability of the ImRSA-optimized TID controller to handle such variations ensures the robustness of the control system under renewable energy integration. Fig. 8 shows the variation in solar radiation applied to the PV system in Area I. Solar radiation fluctuates over time due to environmental factors such as cloud cover, which can cause sudden drops or increases in power generation from the PV grid. These fluctuations must be managed effectively to maintain system stability.

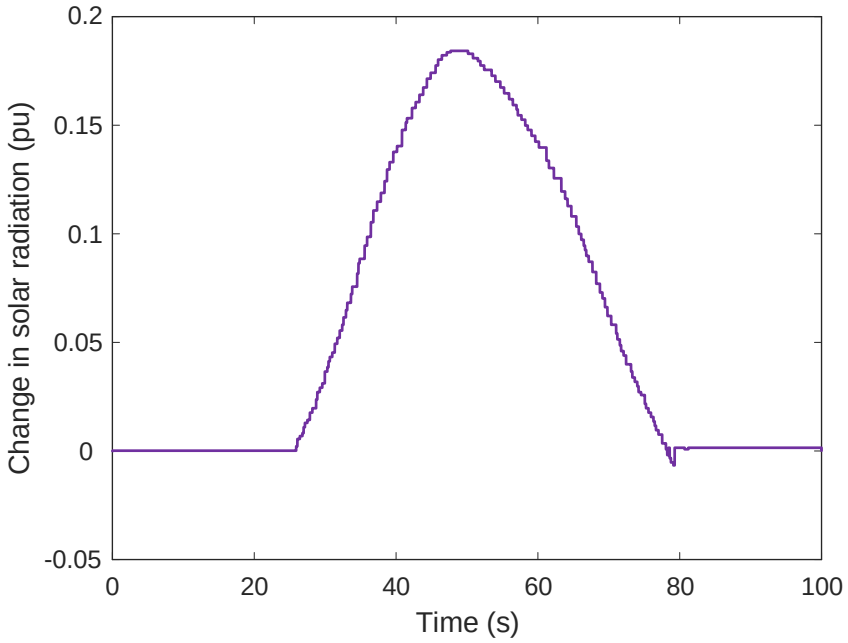

Fig. 8. Change of solar radiation

The transient response of the system, controlled by the ImRSA-optimized TID controller, is illustrated in Fig. 9. This figure displays the frequency deviation in Area I and Area II and the tie-line power deviation between Areas I and II as solar radiation varies. The results indicate that the ImRSA-optimized TID controller successfully mitigates the effects of solar radiation fluctuations on the system's frequency. Despite changes in solar radiation, the frequency deviation in Area I remains within acceptable limits, demonstrating the controller's capacity to maintain system stability under varying power inputs from the PV grid. The tie-line power deviation is also minimized, ensuring that power exchanges between the two areas remain balanced. The ImRSA-optimized TID controller effectively manages the variations in power generated by the PV system, stabilizing the frequencies in Area I and Area II and maintaining the tie-line power flow. This demonstrates the controller's robustness and adaptability in the face of renewable energy integration, where fluctuating energy inputs are common. The ability to handle solar radiation variability without causing significant disturbances in the power system underscores the effectiveness of the ImRSA-optimized TID controller in real-world applications involving renewable energy sources.

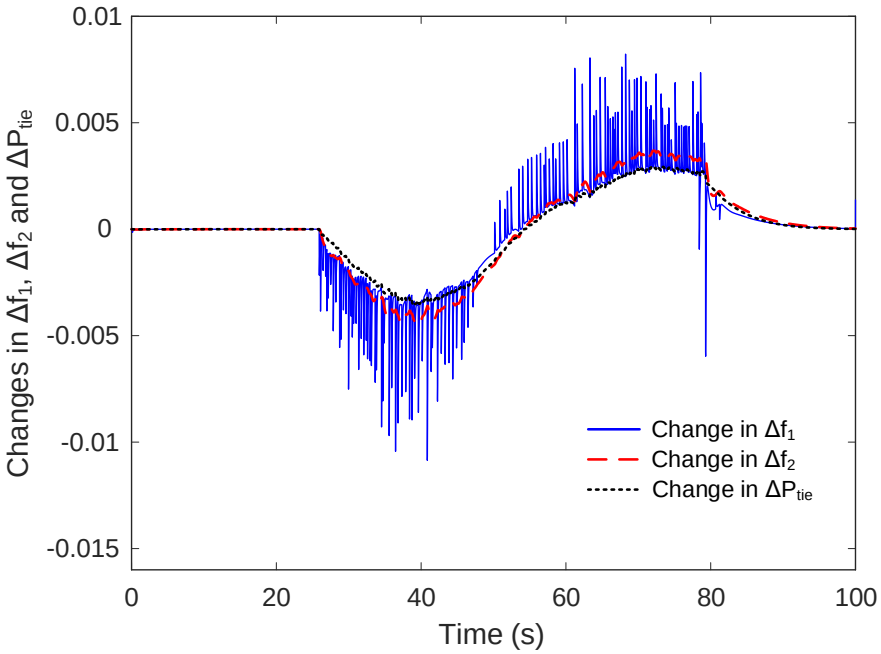

Fig. 9. Transient response of ImRSA-optimized TID controlled system under change of solar radiation

6. Conclusion and Future Works

The ImRSA-optimized TID controller developed in this study demonstrates significant improvements over the original RSA and other optimization techniques in load frequency control for a two-area power system with photovoltaic and thermal power units. By integrating Lévy flight and logarithmic spiral search mechanisms, the ImRSA enhances exploration and convergence, achieving better frequency stabilization and minimizing tie-line power fluctuations under varying load conditions. The simulation results show that the ImRSA-optimized TID controller consistently outperforms RSA, MGWO-CS, BWOA, and GTO in terms of undershoot, overshoot, settling time, and the ITAE objective function, confirming its superiority in terms of both efficiency and robustness. The ImRSA also proves to be highly effective in handling solar radiation variability, stabilizing frequency deviations caused by fluctuating renewable energy sources.

Future work could explore the integration of more advanced hybrid optimization algorithms to further improve the performance of the TID controller. Additionally, the application of the ImRSA in more complex multi-area power systems with a higher level of renewable energy penetration would be a valuable area for research. Moreover, investigating the scalability of the ImRSA for real-time control in large-scale power grids, alongside its adaptation to accommodate other renewable energy

sources such as wind, would broaden the applicability of this approach in modern power system design.

Author Contribution: All authors contributed equally. The final paper was checked and approved by all authors.

Funding: There was no financial support received for this work.

Conflicts of Interest: None of the authors present any conflicts of interest.

References

[1] I. F. Davoudkhani, P. Zare, S. J. S. Shenava, A. Y. Abdelaziz, M. Bajaj, M. B. Tuka, "Maiden application of mountaineering team-based optimization algorithm optimized 1PD-PI controller for load frequency control in islanded microgrid with renewable energy sources," *Scientific Reports*, vol. 14, 2024, https://doi.org/10.1038/s41598-024-74051-x.

[2] T. Ali *et al*., "Terminal Voltage and Load Frequency Control in a Real Four-Area Multi-Source Interconnected Power System With Nonlinearities via OOBO Algorithm," *IEEE Access*, vol. 12, pp. 123782-123803, 2024, https://doi.org/10.1109/ACCESS.2024.3453755.

[3] M. Barakat, "Novel chaos game optimization tuned-fractional-order PID fractional-order PI controller for load–frequency control of interconnected power systems," *Protection and Control of Modern Power Systems*, vol. 7, 2022, https://doi.org/10.1186/s41601-022-00238-x.

[4] P. R. Sahu *et al*., "Effective Load Frequency Control of Power System with Two-Degree Freedom Tilt-Integral-Derivative Based on Whale Optimization Algorithm," *Sustainability*, vol. 15, no. 2, p. 1515, 2023, https://doi.org/10.3390/su15021515.

[5] S. Ekinci, Ö. Can, M. Ş. Ayas, D. Izci, M. Salman and M. Rashdan, "Automatic Generation Control of a Hybrid PV-Reheat Thermal Power System Using RIME Algorithm," *IEEE Access*, vol. 12, pp. 26919-26930, 2024, https://doi.org/10.1109/ACCESS.2024.3367011.

[6] C. Andic, S. Ozumcan, M. Varan, A. Ozturk, "A Novel Sea Horse Optimizer Based Load Frequency Controller for Two-Area Power System with PV and Thermal Units," *International Journal of Robotics and Control Systems*, vol. 4, no. 2, pp. 606-627, 2024, https://doi.org/10.31763/ijrcs.v4i2.1341.

[7] O. Abbaker Ahmed Mohammed *et al*., "Optimal α-Variable Model-Free Adaptive Barrier Function Fractional Order Nonlinear Sliding Mode Control for Four Area Interconnected Hybrid Power System With Nonlinearities," *IEEE Access*, vol. 12, pp. 61586-61609, 2024, https://doi.org/10.1109/ACCESS.2024.3391611.

[8] S. Ekinci, D. Izci, C. Turkeri, M.A. Ahmad, "Spider Wasp Optimizer-Optimized Cascaded Fractional-Order Controller for Load Frequency Control in a Photovoltaic-Integrated Two-Area System," *Mathematics*, vol. 12, no. 19, p. 3076, 2024, https://doi.org/10.3390/math12193076.

[9] A. Sharma, N. Singh, "Load frequency control of connected multi-area multi-source power systems using energy storage and lyrebird optimization algorithm tuned PID controller," *Journal of Energy Storage*, vol. 100, p. 113609, 2024, https://doi.org/10.1016/j.est.2024.113609.

[10] A. T. Hassan *et al*., "Adaptive Load Frequency Control in Microgrids Considering PV Sources and EVs Impacts: Applications of Hybrid Sine Cosine Optimizer and Balloon Effect Identifier Algorithms," *International Journal of Robotics and Control Systems*, vol. 4, no. 2, pp. 941-957, 2024, https://doi.org/10.31763/ijrcs.v4i2.1448.

[11] W. Younis, M.Z. Yameen, A. Tayab, H.G.M. Qamar, E. Ghith, M. Tlija, "Enhancing Load Frequency Control of Interconnected Power System Using Hybrid PSO-AHA Optimizer," *Energies*, vol. 17, no. 16, p. 3962, 2024, https://doi.org/10.3390/en17163962.

[12] S. Ekinci, D. Izci, O. Can, M. Bajaj, V. Blazek, "Frequency regulation of PV-reheat thermal power system via a novel hybrid educational competition optimizer with pattern search and cascaded PDN-PI controller," *Results in Engineering*, vol. 24, p. 102958, 2024, https://doi.org/10.1016/j.rineng.2024.102958.

[13] F. Daneshfar, H. Bevrani, "Multiobjective design of load frequency control using genetic algorithms," *International Journal of Electrical Power & Energy Systems*, vol. 42, no. 1, pp. 257-263, 2012, https://doi.org/10.1016/j.ijepes.2012.04.024.

[14] K. Naidu, H. Mokhlis, A. H. A. Bakar, "Multiobjective optimization using weighted sum Artificial Bee Colony algorithm for Load Frequency Control," *International Journal of Electrical Power & Energy Systems*, vol. 55, pp. 657-667, 2014, https://doi.org/10.1016/j.ijepes.2013.10.022.

[15] I. Pan, S. Das, "Fractional-order load-frequency control of interconnected power systems using chaotic multi-objective optimization," *Applied Soft Computing*, vol. 29, pp. 328-344, 2015, https://doi.org/10.1016/j.asoc.2014.12.032.

[16] B. K. Sahu, T. K. Pati, J. R. Nayak, S. Panda, S. K. Kar, "A novel hybrid LUS–TLBO optimized fuzzy-PID controller for load frequency control of multi-source power system," *International Journal of Electrical Power & Energy Systems*, vol. 74, pp. 58-69, 2016, https://doi.org/10.1016/j.ijepes.2015.07.020.

[17] P. Ojaghi and M. Rahmani, "LMI-Based Robust Predictive Load Frequency Control for Power Systems With Communication Delays," *IEEE Transactions on Power Systems*, vol. 32, no. 5, pp. 4091-4100, 2017, https://doi.org/10.1109/TPWRS.2017.2654453.

[18] M. Gheisarnejad, "An effective hybrid harmony search and cuckoo optimization algorithm based fuzzy PID controller for load frequency control," *Applied Soft Computing*, vol. 65, pp. 121-138, 2018, https://doi.org/10.1016/j.asoc.2018.01.007.

[19] K. Lu, W. Zhou, G. Zeng, Y. Zheng, "Constrained population extremal optimization-based robust load frequency control of multi-area interconnected power system," *International Journal of Electrical Power & Energy Systems*, vol. 105, pp. 249-271, 2019, https://doi.org/10.1016/j.ijepes.2018.08.043.

[20] A. Fathy, A. M. Kassem, "Antlion optimizer-ANFIS load frequency control for multi-interconnected plants comprising photovoltaic and wind turbine," *ISA Transactions*, vol. 87, pp. 282-296, 2019, https://doi.org/10.1016/j.isatra.2018.11.035.

[21] D. Yousri, T.S. Babu, A. Fathy, "Recent methodology based Harris Hawks optimizer for designing load frequency control incorporated in multi-interconnected renewable energy plants," *Sustainable Energy, Grids and Networks*, vol. 22, p. 100352, 2020, https://doi.org/10.1016/j.segan.2020.100352.

[22] A. Latif, S. M. S. Hussain, D. C. Das, T. S. Ustun, "Double stage controller optimization for load frequency stabilization in hybrid wind-ocean wave energy based maritime microgrid system," *Applied Energy*, vol. 282, p. 116171, 2021, https://doi.org/10.1016/j.apenergy.2020.116171.

[23] M. Barakat, A. Donkol, H. F. A. Hamed, G. M. Salama, "Harris Hawks-Based Optimization Algorithm for Automatic LFC of the Interconnected Power System Using PD-PI Cascade Control," *Journal of Electrical Engineering & Technology*, vol. 16, pp. 1845-1865, 2021, https://doi.org/10.1007/s42835-021-00729-1.

[24] N. K. Kumar *et al*., "Fuzzy Logic-Based Load Frequency Control in an Island Hybrid Power System Model Using Artificial Bee Colony Optimization," *Energies*, vol. 15, no. 6, p. 2199, 2022, https://doi.org/10.3390/en15062199.

[25] C. Lu, R. Tang, Y. Chen, C. Li, "Robust tilt-integral-derivative controller synthesis for first-order plus time delay and higher-order systems," *International Journal of Robust and Nonlinear Control*, vol. 33, no. 3, pp. 1566-1592, 2023, https://doi.org/10.1002/rnc.6449.

[26] L. Abualigah, M.A. Elaziz, P. Sumari, Z. W. Geem, A. H. Gandomi, "Reptile Search Algorithm (RSA): A nature-inspired meta-heuristic optimizer," *Expert Systems with Applications*, vol. 191, p. 116158, 2021, https://doi.org/10.1016/j.eswa.2021.116158.

[27] X. Yang and S. Deb, "Cuckoo Search via Lévy flights," *2009 World Congress on Nature & Biologically Inspired Computing (NaBIC)*, pp. 210-214, 2009, https://doi.org/10.1109/NABIC.2009.5393690.

[28] D. Izci, S. Ekinci, E. Eker, M. Kayri, "Augmented hunger games search algorithm using logarithmic spiral opposition-based learning for function optimization and controller design," *Journal of King Saud University - Engineering Sciences*, vol. 36, no. 5, pp. 330-338, 2024, https://doi.org/10.1016/j.jksues.2022.03.001.

[29] Ö. Can, C. Andiç, S. Ekinci, D. Izci, "Enhancing transient response performance of automatic voltage regulator system by using a novel control design strategy," *Electrical Engineering*, vol. 105, pp. 1993-2005, 2023, https://doi.org/10.1007/s00202-023-01777-8.

[30] S. Ekinci, D. Izci, "Enhanced reptile search algorithm with Lévy flight for vehicle cruise control system design," *Evolutionary Intelligence*, vol. 16, pp. 1339-1351, 2023, https://doi.org/10.1007/s12065-022-00745-8.

[31] M. M. Emam, E. H. Houssein, R. M. Ghoniem, "A modified reptile search algorithm for global optimization and image segmentation: Case study brain MRI images," *Computers in Biology and Medicine*, vol. 152, p. 106404, 2023, https://doi.org/10.1016/j.compbiomed.2022.106404.

[32] R. Saravanan, O. Sobhana, M. Lakshmanan, P. Arulkumar, "Fuel cell electric vehicles equipped with energy storage system for energy management: A hybrid JS-RSA approach," *Journal of Energy Storage*, vol. 72, p. 108646, 2023, https://doi.org/10.1016/j.est.2023.108646.

[33] Z. Elgamal, A. Q. M. Sabri, M. Tubishat, D. Tbaishat, S. N. Makhadmeh and O. A. Alomari, "Improved Reptile Search Optimization Algorithm Using Chaotic Map and Simulated Annealing for Feature Selection in Medical Field," *IEEE Access*, vol. 10, pp. 51428-51446, 2022, https://doi.org/10.1109/ACCESS.2022.3174854.

[34] D. Izci, S. Ekinci, "The promise of metaheuristic algorithms for efficient operation of a highly complex power system," *Comprehensive Metaheuristics*, pp. 325-346, 2023, https://doi.org/10.1016/B978-0-323-91781-0.00017-X.

[35] M. Pavlov-Kagadejev *et al*., "Optimizing long-short-term memory models via metaheuristics for decomposition aided wind energy generation forecasting," *Artificial Intelligence Review*, vol. 57, no. 45, 2024, https://doi.org/10.1007/s10462-023-10678-y.

[36] S. Chauhan, G. Vashishtha, A. Kumar, "Approximating parameters of photovoltaic models using an amended reptile search algorithm," *Journal of Ambient Intelligence and Humanized Computing*, vol. 14, pp. 9073-9088, 2023, https://doi.org/10.1007/s12652-022-04412-9.

[37] D. Izci, S. Ekinci, C. Budak and V. Gider, "PID Controller Design for DFIG-based Wind Turbine via Reptile Search Algorithm," *2022 Global Energy Conference (GEC)*, pp. 154-158, 2022, https://doi.org/10.1109/GEC55014.2022.9986617.

[38] M. Maashi *et al*., "Modeling of Reptile Search Algorithm With Deep Learning Approach for Copy Move Image Forgery Detection," *IEEE Access*, vol. 11, pp. 87297-87304, 2023, https://doi.org/10.1109/ACCESS.2023.3304237.

[39] S. Ekinci, D. Izci, L. Abualigah, R. Ghandour and M. Salman, "Prairie Dog Optimization-based Tilt-Integral-Derivative Controller for Frequency Regulation of Power System," *2024 8th International Artificial Intelligence and Data Processing Symposium (IDAP)*, pp. 1-6, 2024, https://doi.org/10.1109/IDAP64064.2024.10710671.

[40] S. Ekinci, D. Izci, L. Abualigah, A. G. Hussien, C. Thanh, S. Khatir, "Revolutionizing Vehicle Cruise Control: An Elite Opposition-Based Pattern Search Mechanism Augmented INFO Algorithm for Enhanced Controller Design," *International Journal of Computational Intelligence Systems*, vol. 16, no. 129, 2023, https://doi.org/10.1007/s44196-023-00304-8.

[41] R. K. Khadanga, A. Kumar, S. Panda, "A modified Grey Wolf Optimization with Cuckoo Search Algorithm for load frequency controller design of hybrid power system," *Applied Soft Computing*, vol. 124, p. 109011, 2022, https://doi.org/10.1016/j.asoc.2022.109011.

[42] P. Dahiya and A. K. Saha, "Frequency Regulation of Interconnected Power System Using Black Widow Optimization," *IEEE Access*, vol. 10, pp. 25219-25236, 2022, https://doi.org/10.1109/ACCESS.2022.3155201.

[43] O. Can, M. S. Ayas, "Gorilla troops optimization-based load frequency control in PV-thermal power system," *Neural Computing and Applications*, vol. 36, pp. 4179-4193, 2024, https://doi.org/10.1007/s00521-023-09273-7.

[44] S. Ekinci, D. Izci, B. Hekimoglu, "Implementing the Henry Gas Solubility Optimization Algorithm for Optimal Power System Stabilizer Design," *Electrica*, vol. 21, no. 2, pp. 250-258, 2021, https://doi.org/10.5152/electrica.2021.20088.

[45] D. Izci, S. Ekinci, S. Mirjalili, L. Abualigah, "An intelligent tuning scheme with a master/slave approach for efficient control of the automatic voltage regulator," *Neural Computing and Applications*, vol. 35, pp. 19099-19115, 2023, https://doi.org/10.1007/s00521-023-08740-5.

[46] S. Ekinci, D. Izci, R. Abu Zitar, A. R. Alsoud, L. Abualigah, "Development of Lévy flight-based reptile search algorithm with local search ability for power systems engineering design problems," *Neural Computing and Applications*, vol. 34, pp. 20263-20283, 2022, https://doi.org/10.1007/s00521-022-07575-w.

[47] E. Eker, M. Kayri, S. Ekinci, D. Izci, "A New Fusion of ASO with SA Algorithm and Its Applications to MLP Training and DC Motor Speed Control," *Arabian Journal for Science and Engineering*, vol. 46 pp. 3889-3911, 2021, https://doi.org/10.1007/s13369-020-05228-5.

[48] Y. Lv, W. Liu, Y. Zheng, S. Chen, Q. Chen, "Start-up process optimization of pumped-storage unit with Tilt–Integral–Derivative controller," *Transactions of the Institute of Measurement and Control*, vol. 45, no. 9, pp. 1781-1794, 2023, https://doi.org/10.1177/01423312221147551.

[49] D. Izci, S. Ekinci, "Optimizing Three-Tank Liquid Level Control: Insights from Prairie Dog Optimization," *International Journal of Robotics and Control Systems*, vol. 3, no. 3, pp. 599-608, 2023, https://doi.org/10.31763/ijrcs.v3i3.1116.

[50] L. K. Fong, M. S. Islam, M. A. Ahmad, "Optimized PID Controller of DC-DC Buck Converter based on Archimedes Optimization Algorithm," *International Journal of Robotics and Control Systems*, vol. 3, no. 4, pp. 658-672, 2023, https://doi.org/10.31763/ijrcs.v3i4.1113.

[51] L. Abualigah, S. Ekinci, D. Izci, "Aircraft Pitch Control via Filtered Proportional-Integral-Derivative Controller Design Using Sinh Cosh Optimizer," *International Journal of Robotics and Control Systems*, vol. 4, no. 2, pp. 746-757, 2024, https://doi.org/10.31763/ijrcs.v4i2.1433.

[52] V. Snášel, R. M. Rizk-Allah, D. Izci, S. Ekinci, "Weighted mean of vectors optimization algorithm and its application in designing the power system stabilizer," *Applied Soft Computing*, vol. 136, p. 110085, 2023, https://doi.org/10.1016/j.asoc.2023.110085.